ACSNANO

www.acsnano.org

ARTICLE

High-Electrification Performance and Mechanism of a Water–Solid Mode Triboelectric Nanogenerator

Jing You,[#] Jiajia Shao,[#] Yahua He,[#] Frank Fei Yun, Khay Wai See,* Zhong Lin Wang,* and Xiaolin Wang*

Cite This: https://doi.org/10.1021/acsnano.1c00795

Read Online

ACCESS | Metrics & More | Article Recommendations | Supporting Information

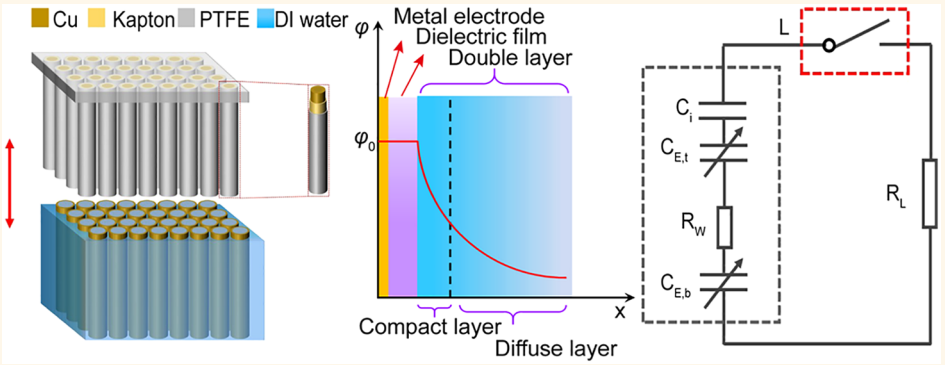

ABSTRACT: With the advantages of superior wear resistance, mechanical durability, and stability, the liquid–solid mode triboelectric nanogenerator (TENG) has been attracting much attention in the field of energy harvesting and self-powered sensors. However, most reports are primarily observational, and there still lacks a universal model of this kind of TENG. Here, an equivalent circuit model and corresponding governing equations of a water–solid mode TENG are developed, which could easily be extended to other types of liquid–solid mode TENGs. Based on the first-order lumped circuit theory, the full equivalent circuit model of water–solid mode TENG is modeled as a series connection of two capacitors and a water resistor. Accordingly, its output characteristics and critical influences are examined, to investigate the relevant physical mechanism behind them. Afterward, a three-dimensional water–solid TENG array constructed from many single-wire TENGs is fabricated, which can not only harvest tiny amounts of energy from any movement of water, but also can verify our theoretical predictions. The fundamentals of the water–solid mode TENG presented in this work could contribute to solving the problem of electrical phenomena on a liquid–solid interface, and may establish a sound basis for a thorough understanding of the liquid–solid mode TENG.

KEYWORDS: *triboelectric nanogenerator, water–solid mode TENG, water–solid interface, electrical double layer, Wang's hybrid layer*

INTRODUCTION

Researchers have attempted to understand and utilize contact electrification (CE) for many centuries.[1−4] CE occurring at liquid–solid interfaces usually endows the liquid (water or an aqueous solution) with specific electric charges, which accordingly leads to the formation of an electrical double layer (EDL) within the fluid.[5−8] A well-known example is that when the water surface is broken or brought into contact with a solid, electric charges are generated on the interfaces, and an EDL is formed in this complex system. Recently, it has been proposed that there are two steps, including the electron exchange and ion adsorption, for the generation of an EDL, which will be comprehensively researched in the foreseeable future. This two-step model is called the Wang model for EDL,

Received: January 28, 2021
Accepted: April 26, 2021

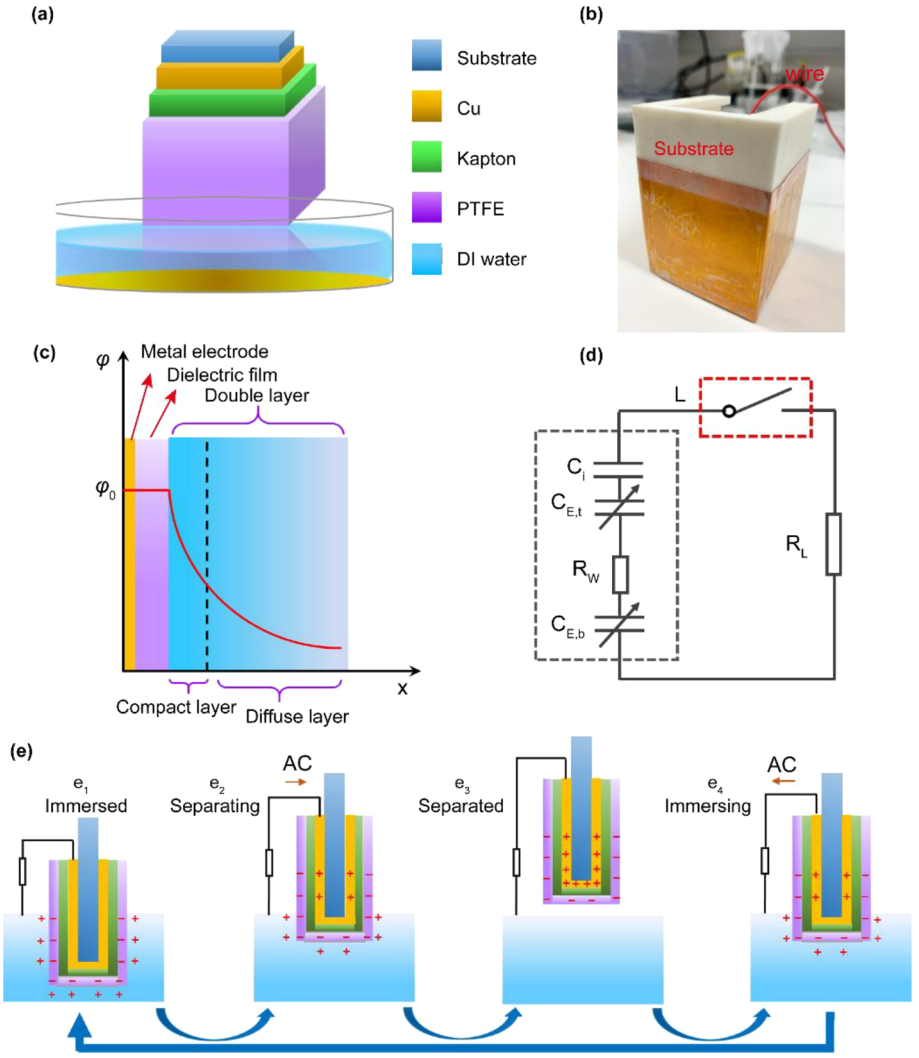

Figure 1. (a) Schematic diagram of the water−solid triboelectric nanogenerator and (b) photograph of the moving part setup. (c) Typical electrical double layer formed on the water−dielectric interface area and the relevant variation of electrostatic potential (φ) with distance x from the electrode. (d) The full equivalent circuit model of the water−solid triboelectric nanogenerator. (e) Step-by-step illustration showing the working principle of the water−solid mode triboelectric nanogenerator.

and the relevant hybrid layer is called Wang's hybrid layer.[9−11] On the other hand, CE occurring at water−solid interfaces is utilized to harvest energy in the small-scale energy range from macroscopic to microfluidic devices.[12−17] Moon et al. has demonstrated that mechanically changing the contact area at the liquid−solid interface essentially modulates the electrical double layer, thereby generating an electrical current.[7] In a recently study by Xu and Wang et al., it was found that spreading of a water droplet on an electric generator gains an enhancement to its instantaneous power density.[12] However, this type of small-scale energy harvesters have to overcome inevitable difficulties in actual applications, such as water evaporation, water splashing, or extremely small instantaneous currents generated under a low frequency.[14,15]

To overcome the above problems, a special energy harvesting device, that is, the water−solid mode triboelectric nanogenerator (TENG) has been designed, which can improve the basic output by several orders of magnitude over the droplet-based devices as mentioned above. This is mainly because a droplet is replaced by great quantities of water, which leads to the increase in contact area, making the interfacial effect more obvious. For instance, a highly symmetric three-dimensional (3D) spherical-shaped water-based TENG was designed by Shi et al., which can be effectively utilized to harvest energy from water waves with random direction/amplitude because its inner surface and outer surface are in direct contact with the water.[18] To date, a large number of water-based mode TENGs have been invented,[16,17] owing to the great advantages of this type of TENG, such as superior wear resistance, good mechanical durability, and stability, etc.[19−23] These consistent reports are primarily observational, however, and they are generally difficult to reproduce, especially because no universal model has been developed.

In this work, we have achieved a comprehensive understanding of the physical mechanisms of the water−solid mode TENG, through our equivalent circuit model and clear physical picture. First, the EDLs and corresponding EDL capacitors (EDLCs) formed on the water−solid interfacial areas are systematically analyzed. The two EDLCs and the resistance of the water are connected in series, from which a full equivalent circuit model and governing equation are proposed, based on the first-order lumped-circuit theory. On mechanically modulating the EDLs, the voltages across the EDLCs and

https://doi.org/10.1021/acsnano.1c00795
ACS Nano XXXX, XXX, XXX−XXX

the potential difference between the two electrodes change, consequently giving rise to the generation of a conduction current in the external circuit. In addition, a three-dimensional water−solid mode TENG array constructed from many single-wire TENGs is fabricated, which can not only convert energy from any movement of water, but also verify our predictions and theoretical analysis.

RESULTS AND DISCUSSION

The typical water−solid mode TENG comprises of a multidielectric layer constructed from polyimide (Kapton) tape and polytetrafluoroethylene (PTFE) films, deionized (DI) water, and two electrodes. Figure 1a shows a simple schematic diagram of this device, from which it is seen that the PTFE (hydrophobic) surface is directly exposed to DI water. A picture of the substrate attached with the multidielectric layer is presented in Figure 1b. When CE first occurs between the DI water and the PTFE, negative charges are generated on the hydrophobic surface and positive charges on the water surface (Figure 1e). Identifying the origins of the charges on water−hydrophobic interfaces is inherently challenging, owing to the uncertainties in their interfacial structures and known surface chemistry. Here, we accept the postulate that hydroxyl ion adsorption is the source of charge on hydrophobic surfaces and that EDLs are formed at the liquid−solid interfaces.[24] As shown in Figure 1e, the negative charges distributed on the PTFE surface generate an electric field, pulling oppositely charged ions toward this hydrophobic surface and pushing like charges away from it. Since the opposite electric charges (counterions) are distributed very near the PTFE surface, they then shield the water solution from those negative charges. According to the charge neutrality condition, the total charge is zero, but the dipole moment close to the interface region is not zero. This charge distribution structure in the fluid is well-known as the EDL or the Debye layer.[25] Because the geometry and structure of the charge distribution is equivalent to that of a conventional parallel plate capacitor, it is regarded as an electrical double layer capacitor (EDLC), as depicted in Figure 1c. There are two different EDLCs formed in the water−solid mode TENG, with the one distributed at the water−PTFE surface, while the other is formed at the water−bottom electrode surface.

Figure 1c illustrates the modeled EDL and EDLC in the water−solid mode TENG. Note that the double layer is formed by a compact layer of charges next to the charged surface (PTFE) followed by a diffuse layer extending into bulk solution (DI water). We assume that the capacitance near the water-PTFE surface (C_{top}) is comprised of two capacitors, C_i and $C_{EDLC,t}$, which are connected in series form. The C_i and $C_{EDLC,t}$ represent the capacitance of the dielectric and the EDLC formed at the water-PTFE interfacial area, respectively. It should be emphasized that the C_{top} is a nonlinear capacitor due to the change in the $C_{EDLC,t}$. Strictly speaking, this $C_{EDLC,t}$ is a typical voltage-dependent capacitor, and its capacitance is regarded as a differential capacitance, which can be calculated by the rate of the stored charge divided by the rate of change of the voltage across the EDLC. As the free charges distributed on the surface of the top electrode vary with time, the total electric field applied on the water−PTFE surface changes, leading to variation in the charges distributions in both the compact layer and the diffuse layer, and the length of the relevant EDL. Therefore, the $C_{EDLC,t}$ and C_{top} all change with time. By the same token, the $C_{EDLC,b}$ that is formed at the water−bottom electrode interfacial area is also a typical differential capacitor. Two points should be noted. The first one is about the fundamental basic of charge generation on the liquid−solid interfaces. It has been proposed by Wang that electron exchange between the liquid (water) and the solid (PTFE film) at the interface is an inevitable step when CE occurs, which can be described by an overlapped electron cloud model between water molecules and solid surface atoms.[25,26] In particular, electron transfer and ion adsorption usually happen simultaneously. Furthermore, it is apparent that the EDLCs (including the $C_{EDLC,t}$ and $C_{EDLC,b}$) can be mechanically modulated under different structure parameters and motion conditions.

Based on the above analysis, a full equivalent circuit model of the water−solid mode TENG is proposed. As demonstrated in Figure 1d, the TENG is modeled by a series connection of C_i, $C_{EDLC,t}$, R_w, and $C_{EDLC,b}$, where C_i represents the time-invariant capacitance caused by the dielectric material such as nylon or PTFE. R_w is the resistance of water (the liquid).[7] Before the moving part comes into contact with water, there is a capacitance from the environment. Given that this capacitor is fairly small, it is regarded existing in at an open circuit condition, and is represented by a switch L. Moreover, R_L represents the external resistance in the external circuit. Assume that the contact area (S_w) between the water and the PTFE changes appreciably during external mechanical excitation. While the contact area (S_b) between the water and the bottom electrode is nearly fixed, the moving part moves up and down within the water. As a result, the total capacitance at the water-PTFE interface C_{top} is approximately proportional to S_w; on the contrary, the capacitance formed at the bottom electrode-water surface (C_{bot}, which is equal to the $C_{EDLC,b}$ in this device structure) is nearly a constant during the oscillation period. It should be clear that the thus-formed EDLC is much smaller than that of the dielectric capacitance in general,[13] and these capacitors are connected in series, so that the $C_{EDLC,t}$ can be negligible when calculating the total capacitance. Then, we have (Supporting Information (SI) Note 1),

$$C_{top}(t) = \left(\frac{1}{C_i} + \frac{1}{C_{EDLC,t}}\right)^{-1} = \varepsilon_0 S_w(t)\left(d_0 + \frac{\lambda_w}{\varepsilon_w}\right)^{-1} \cong \frac{\varepsilon_0 S_w(t)}{d_0} \quad (1)$$

$$C_{bot} \cong \frac{\varepsilon_0 \varepsilon_w S_b}{\lambda_w} \quad (2)$$

where d_0 represents the effective thickness of the multidielectric layer, that is, $d_0 = d_1/\varepsilon_1 + d_2/\varepsilon_2$, where d_1, d_2, and ε_1, ε_2 are the thickness and relative permittivity of the Kapton and PTFE, respectively. The λ_w and ε_w are the width of the $C_{EDL,t}$ and the dielectric constant of water, respectively. In most cases, $d_0 \gg \lambda_w/\varepsilon_w$, and the second approximation in eq 1 can be justified. This is the essential reason why eq 1 can be further simplified (SI Note 1). Therefore, variation of C_{top} mainly comes from the changes of effective thickness of the multidielectric layer d_0, while for C_{bot} it depends critically on the thickness of electrical double layer λ_w.

Figure 1e illustrates the charge transfer process in an operation cycle of the water−solid mode TENG. It should be noticed that negative charges are generated on the PTFE surface, and this charged layer remains constant even after the contact surfaces are completely separated owing to the electronegative characteristics of PTFE. As depicted in Figure 1e_1, when the moving part is immersed in water, the electrons

https://doi.org/10.1021/acsnano.1c00795
ACS Nano XXXX, XXX, XXX−XXX

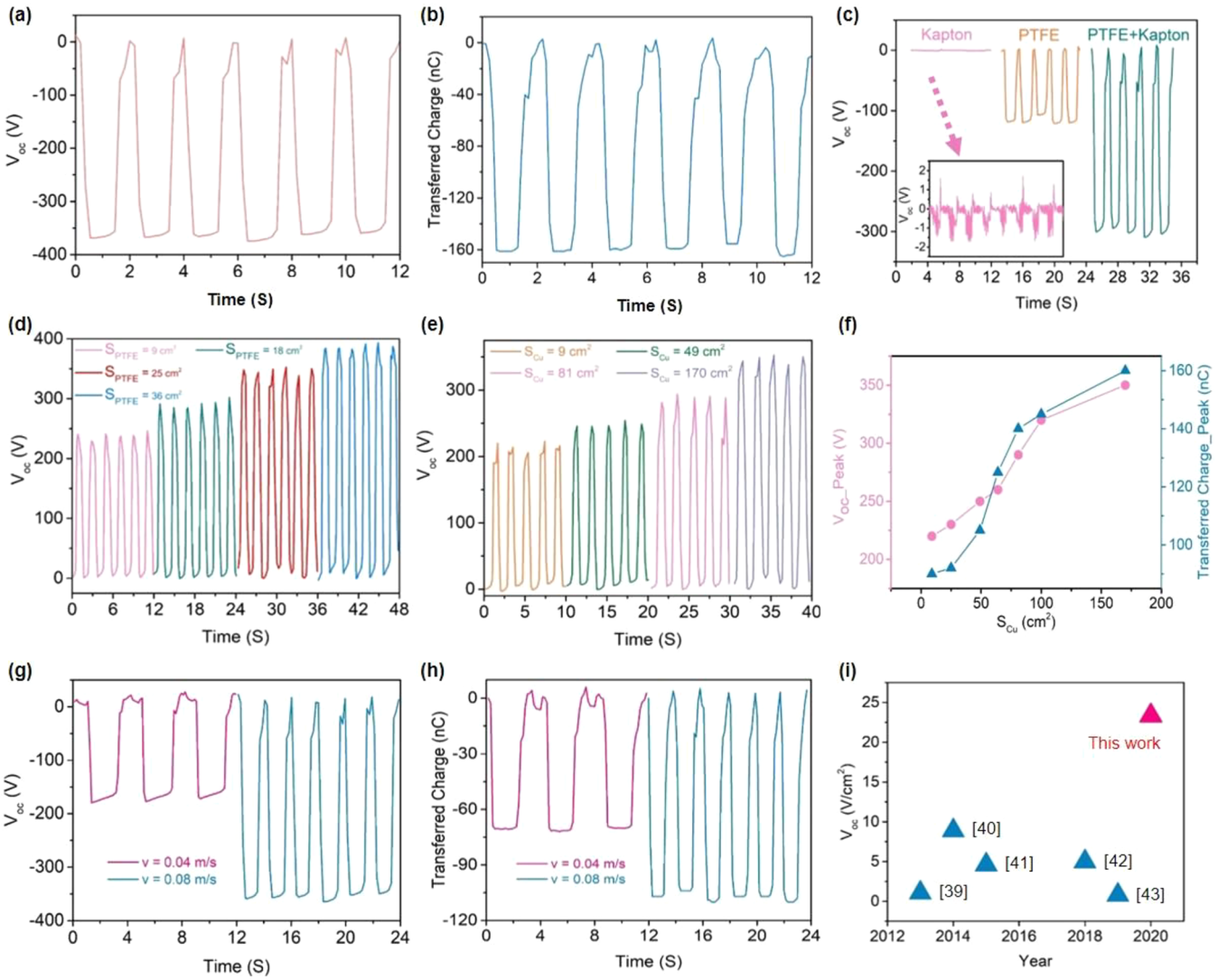

Figure 2. (a) Open-circuit voltage (V_{OC}) and (b) short-circuit transferred charges (Q_{SC}) of the water−solid triboelectric nanogenerator when the areas of the PTFE and Cu are 25 cm^2 and 170 cm^2, respectively. Comparison of the V_{OC} for different (c) material selections, (d) sizes of PTFE, (e) sizes of the bottom electrode. (f) Extracted peaks of V_{OC} and Q_{SC} for different sizes of the bottom electrode. Basic outputs of the (g) V_{OC} and (h) Q_{SC} for different velocities of the moving part. (f) Comparison of the open-circuit voltage densities reported in recent years. Note that the V_{OC} of this work exhibits the largest value.

are injected from the water surface to the PTFE surface, making the contact surfaces oppositely charged. As the TENG is separated from the water, negative charges remains distributed on the surface of PTFE, which leads to the electric potential of the moving electrode lower than that of the bottom electrode, causing the charges transferred between the two electrodes to maintain electrostatic equilibrium (Figure 1e$_2$). The generated conduction current in the external circuit keeps flowing until the moving electrode is completely taken out (Figure 1e$_3$) of DI water. As the moving part comes into contact with the DI water (Figure 1e$_4$) again, the charged PTFE surface will be screened due to the formation of EDL at the water−PTFE interface; charges flow from the bottom electrode to the top one, and the counterions in the DI water (liquid) have to redistribute themselves simultaneously to eliminate the potential difference between the two EDLCs ($C_{EDL,t}$ and $C_{EDL,b}$). As a result, alternating current (AC) is generated in the external circuit. When no electrons are transferred, the voltage between the two EDLCs becomes zero, and the system reaches at an equilibrium state. According to Kirchhoff's law, we have

$$\frac{S_b\sigma_b - Q}{C_{bot}} - \frac{Q}{C_{top}} = 0 \tag{3}$$

here σ_b is the charge density distributed at the bottom electrode, and Q is the decrement or increment of charges in the $C_{EDL,b}$ or $C_{EDL,t}$ in the equilibrium state. In such state, since the C_{bot} is much larger than the C_{top} in most cases (SI Note 1), the electric charges distributed in the top EDLC should be much smaller than those distributed in the bottom EDLC. As a result, the potential difference between the two EDLCs is strongly depended on the time-variation of C_{top}. In the nonequilibrium state, assume that the charges stored on C_{top} and C_{bot} are $Q_{top} + Q$ and $S_b\sigma_T - Q$, and that the voltage across each EDLC is φ_{top} and φ_{bot}, respectively. The voltage difference (V) between the two electrodes of the water−solid mode TENG is given by Kirchhoff's law:

https://doi.org/10.1021/acsnano.1c00795
ACS Nano XXXX, XXX, XXX−XXX

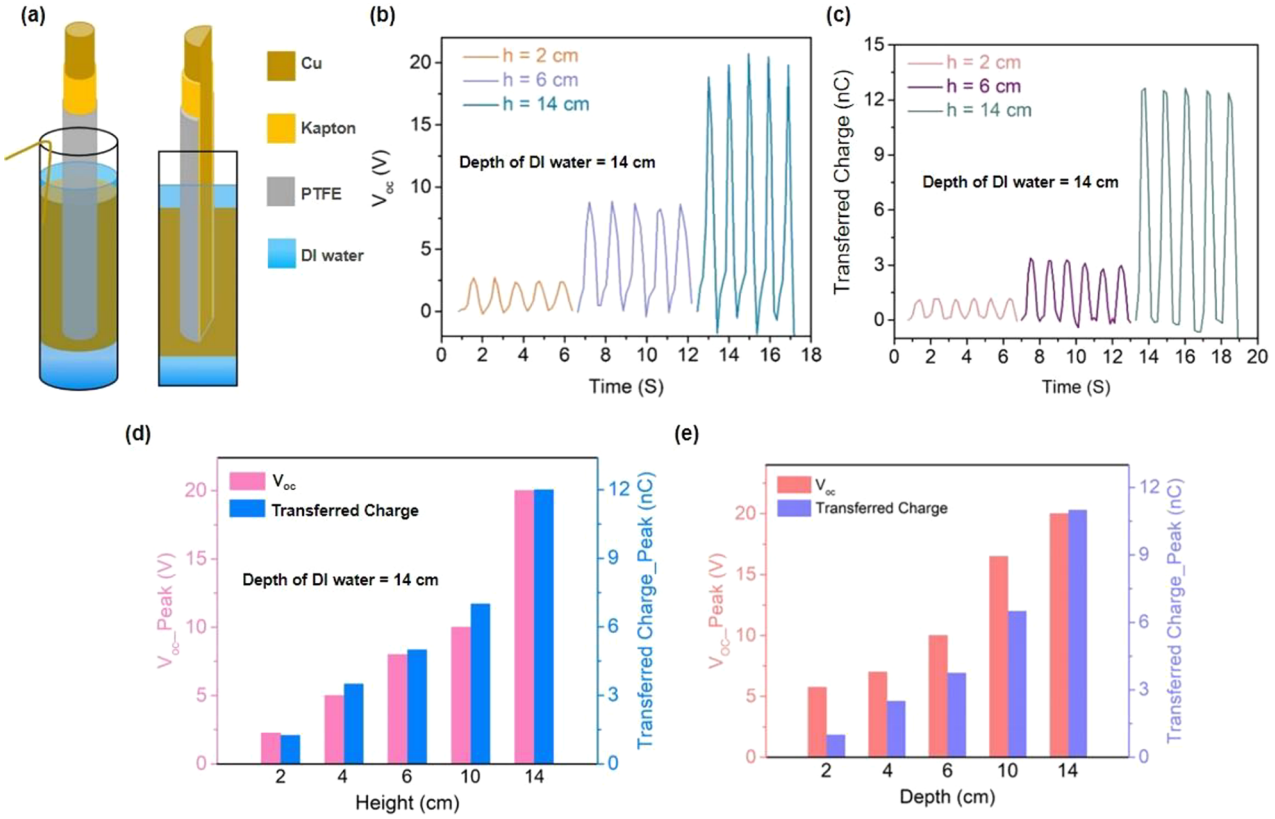

Figure 3. (a) Schematic diagram of the single-wire TENG. Comparison of the (b) V_{OC} and (c) Q_{SC} of the single-wire TENG with increasing immersion length, and (d) corresponding extracted peaks of V_{OC} and Q_{SC}; Note that the depth of DI water is fixed at 14 cm. (e) Extracted peaks of V_{OC} and Q_{SC} at different depths of the DI water.

$$\frac{S_b\sigma_b - Q}{C_{bot}} - \frac{Q_{top} + Q}{C_{top}} - R_w\frac{dQ}{dt} - R_L\frac{dQ}{dt} = 0 \tag{4}$$

and the governing equation can be simplified as

$$(R_L + R_w)\frac{dQ}{dt} = -\left(\frac{1}{C_{bot}} + \frac{1}{C_{top}(t)}\right)Q + \left(\frac{S_b\sigma_b}{C_{bot}} - \frac{Q_{top}}{C_{top}(t)}\right) \tag{5}$$

where $Q(t)$ is the transferred charge. Accordingly, the time-dependent on C_{top} and the nearly constant of C_{bot} make this governing equation to be a nonlinear first-order ordinary differential equation; giving rise to the difficulty of obtaining the analytical solution. If the voltage across the R_L is V_L, it is obtained by

$$V_L = \frac{VR_L}{R_L + R_w} \tag{6}$$

On the other hand, it has been proved that the solid−solid mode TENG is neutral at any time, and this is the essential reason why it is equivalent to an open circuit voltage (V_{OC}) connected in series with a variable capacitor.[27−31] For the water−solid mode TENG, its full equivalent circuit model is modeled as a series connection of two capacitors C_{bot} and C_{top}, and a water resistor R_w. Through mechanically modulating the two EDLs along with the interfacial areas, mechanical work is converted into electrical energy. Some works have been published to demonstrate the exploitation of EDLC for energy conversion.[32,33] In addition, we have proved that the total capacitance of this mode TENG is approximately in the same order when compared with a typical value of the capacitance of a lateral-slide mode TENG (SI Note 1).[34]

To investigate the effects of key parameters and the relevant physical mechanism behind them, the open-circuit voltage $V_{OC}(t)$, short-circuit transfer charge $Q_{SC}(t)$, and total capacitance $C(t)$ are derived according to eq 5 (SI Note 2):

$$V_{OC}(t) = \frac{S_b\sigma_b}{C_{bot}} - \frac{\sigma_w d_0}{S_w} \tag{7}$$

$$Q_{SC}(t) = \frac{S_b\sigma_b - \sigma_w d_0 C_{bot}/\varepsilon_0}{1 + C_{bot}/C_{top}} \tag{8}$$

$$C(t) = \frac{\varepsilon_0\varepsilon_w}{\lambda_w/S_b + d_0\varepsilon_w/S_w} \tag{9}$$

From eqs 7−9, the basic outputs of the water−solid mode TENG can be quantitatively predicted. In addition, we have already pointed out that nanogenerators use displacement current as the driving force to convert mechanical energy into electric power/signals.[3,28,29] This definition also applies to the liquid−solid model TENGs from the first-principles of classical electrodynamics. In other words, the output characteristic of the water−solid mode TENG is controlled by the Maxwell's displacement current (I_D). All-around analysis and simulation of this problem will be developed in our next work.

The basic outputs of the water−solid mode TENG are illustrated in Figure 2. The peak V_{OC} shown in Figure 2a is approximately 375 V, which is more than twice the V_{OC} reported in ref 12 and also is several orders of magnitude larger than that of the droplet device designed by Moon et al.[7]

https://doi.org/10.1021/acsnano.1c00795
ACS Nano XXXX, XXX, XXX−XXX

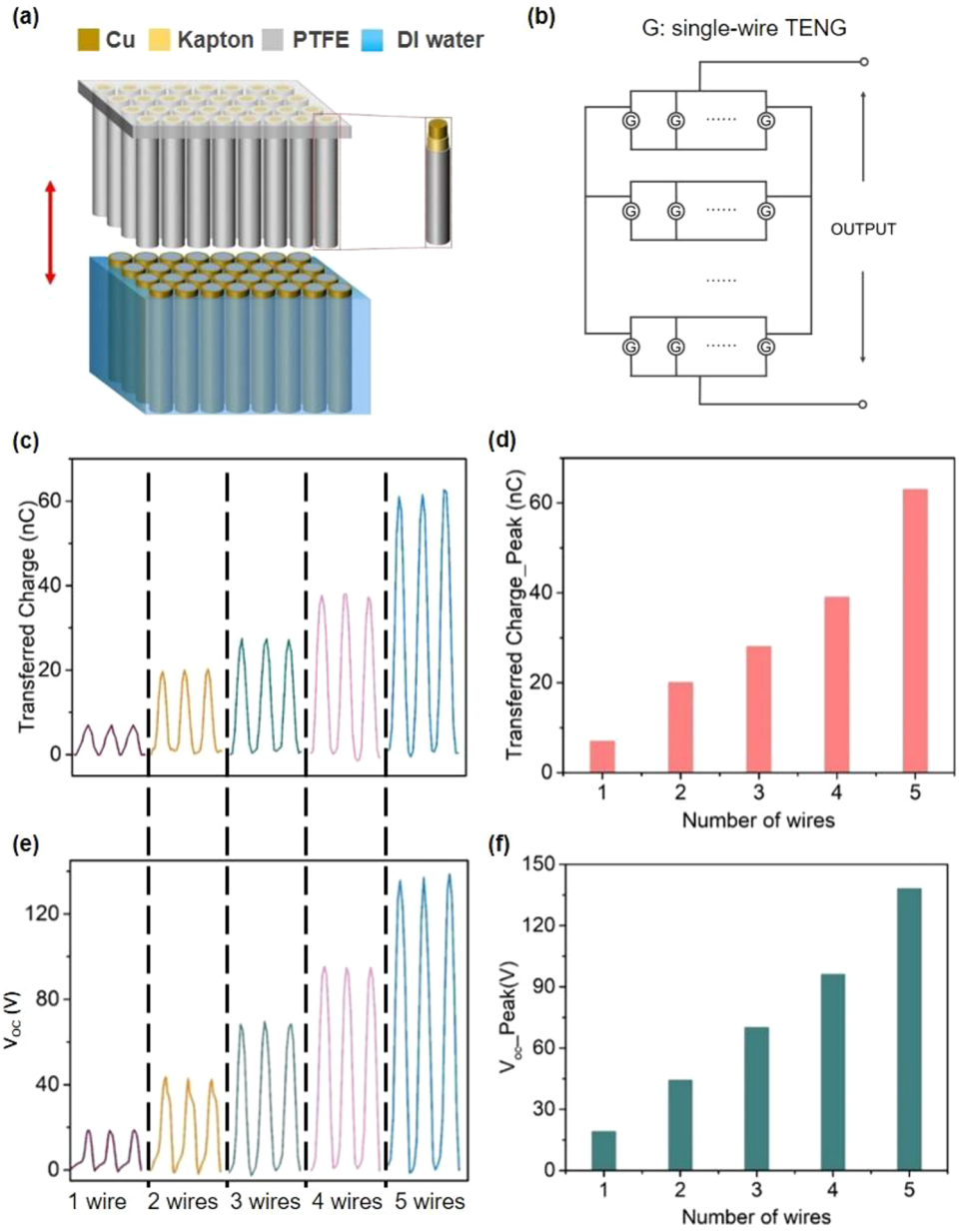

Figure 4. (a) Schematic diagram of the three-dimensional water−solid TENG array, constructed from many single-wire TENGs. (b) The equivalent circuit model of the TENG array. (c,d) Transferred charges Q_{SC} and the extracted peaks of Q_{SC} enhancement with the increase of the integrated wire number. (e-f) Open circuit voltage V_{OC} and the extracted peaks of V_{OC} with the increase of the integrated wire number.

It is apparent that the peak Q_{SC} (Figure 2b) is as high as 160 nC. In the case of the droplet device, its outputs are usually limited by the capillary length of the water bridge formed between the contact surfaces or the interfacial effects.[35] Moreover, it has been proved that the electrical performance of a general solid−solid mode TENG is strongly affected by a group of factors, such as the device configuration, structure parameters, operation conditions, etc.[28,36,37] These conclusions are also applicable to the liquid−solid mode TENGs. As illustrated in Figure 2c, the V_{OC} of the water−solid mode TENG is greatly enhanced when the multidielectric layer is utilized; but similar results cannot be achieved by the utilization of either the Kapton tape or the PTFE film. This is attributed to the larger effective thickness of the multidielectric layer (d_0), that is, increasing the d_0 results in a bigger V_{OC}. Note that the hydrophobic material PTFE leads to a higher output voltage primarily because of its high charge-generation capability.[38]

The results presented in Figures 2d−f show that increasing the contact area improves the V_{OC} and Q_{SC}, which can be proved quantitatively using eqs 7 and 8. For instance, either increasing the L or the $x(t)$ in eq 7 generates a larger V_{OC}. Apart from the contact area, the improvement of the relative velocity can enhance the basic outputs as well (Figures 2g,h). Assume that the moving part is driven with a typical sinusoidal motion and that the $x(t)$ is described in the model via: $x(t) = x_{max}/2/(1 - \cos \omega t)$, where x_{max} and ω represent the largest relative movement and angular frequency, respectively. It is easily found that the V_{OC} (and Q_{SC}) are functions of the velocity. A larger velocity results in a larger moving distance, and then the contact area at the water−PTFE interface is increased at the same time, so that many more charges are

https://doi.org/10.1021/acsnano.1c00795
ACS Nano XXXX, XXX, XXX−XXX

transported between the two electrodes. It should be clear, however, that the surface charge density at the water−PTFE interface is approximately 10 $\mu C/m^2$, which is significantly lower than that for the EDL (50 mC/m^2) reported by Wu et al.[13] In other words, although the formation of negative charge is observed on the hydrophobic surface in our experiment, the number of charges participating in transport is smaller than the available charges at the EDL. Hence, extracting more charges from the EDL to participate in the transport in the external circuit should be the focus of attention on in the next step of the work. Figure 2f presents a comparison of the V_{OC} densities reported in recent years, from which it is seen that the V_{OC} density of this work exhibits the largest value.[39−43]

Using the advantages of the water−solid mode TENG, a single-wire geometric structure device was designed. As demonstrated in Figure 3a, a single Cu wire with a diameter of 2 mm was utilized as one electrode. When the moving part constructed from the Cu wire and the multidielectric layer moves up and down in the DI water in a tube, leading to the generation of conduction current in the external circuit. Since there is no substrate, this method reduces the size and weight of the TENG, and thus improves the system's volume utilization. Although only very little DI water is stored in the tube, excellent outputs are observed in Figures 3b,c. As the immersion depth (represented by h) becomes gradually larger from 2 to 14 cm, the V_{OC} and Q_{SC} increase simultaneously, owing to the increase in the contact area between the water and the PTFE surface. Furthermore, there is nearly a linear relationship between the V_{OC} (and Q_{SC}) and the immersion depth (Figure 3d), and the similar phenomena can be found from the corresponding density of V_{OC} and Q_{SC} (SI Figure S1), from which a type of self-powered displacement sensor could be fabricated and applied in practical applications. It should be noticed that the depth of DI water is fixed closely to14 cm in above-mentioned tests. Interestingly, we can observe the same phenomenon when the depth of DI water changing from 2 to 14 cm, as demonstrated in Figure 3e and SI Figure S2. As proved before, it is mainly because increasing the contact area contributes to the transport of more charges in the external circuit. Developing a set of experimental systems for dynamic measurements based on a special displacement sensor should be investigated in future studies. In particular, we have further noted that when the DI water moved only an extraordinarily small distance, a highly visible signal was obtained in the experiment, implying favorable precision and sensitivity of the device.

Furthermore, a three-dimensional water−solid TENG array comprising many single-wire TENGs was fabricated, which can be utilized as an energy harvester to convert mechanical energy from micro to macro levels, or a self-powered sensor to detect static and dynamic processes through the voltage or current signals. As illustrated in Figure 4a, a large number of single-wire TENGs are connected in parallel to construct the three-dimensional TENG array. Its equivalent circuit model is proposed in Figure 4b, where the single-wire TENG is designated by the letter G. We note that although the basic output of the TENG array is approximately proportional to the number of single wires (Figures 4c,e), which is very obvious from the extracted peaks of V_{OC} and Q_{SC} (Figures 4d,f), it is almost impossible to obtain a very exact association between the number of wires and basic outputs due to the nonlinear variation of the total capacitance of this TENG energy harvesting system. But it suggests that the single-wire TENG exhibits a high scalability for constructing a TENG array, and offers the possibility of integrating and directly powering various functional sensors. On the other hand, due to the easily deformed nature of water, the TENG array system is flexible enough to absorb and convert every water movement while accommodating each small vibration from external mechanical triggering. For the better understanding of the TENG operation, optical photos and videos of the single-wire TENG and the three-dimensional TENG array are provided to show the behavior of water movement and the TENG in energy harvesting situation (SI Figures S3 and S4, and SI movies). Briefly speaking, connecting many single-wire TENGs together can effectively improve the electrical output.

CONCLUSIONS

In summary, an equivalent circuit model of a water−solid mode TENG is proposed, which allow us to have a better understanding about the physical mechanism of this typical energy harvesting device. First, it was found that EDLs and EDLCs are formed on the water−solid interfaces, which includes the water−PTFE interface and the water−electrode interface. Then a full equivalent circuit model of the water−solid mode TENG is built by a series connection of the two EDLCs and the water resistor, according to the lumped-circuit theory. The EDLC is essentially a nonlinear capacitor with voltage-dependent capacitance, making it arduous to analytically solve the TENG's governing equation, but it is still an attractive option for us to quantitatively predict the energy harvesting process. Furthermore, the influences of structure parameters and operation conditions on the electrical response have been investigated directly, by which the relevant physical mechanism behind them are in depth discussed. The results suggest that selecting suitable materials, increasing the contact area, and increasing the velocity are beneficial to improve the basic output. On the other hand, a three-dimensional water−solid TENG array comprising many single-wire TENGs was designed. This special TENG array can not only convert the tiny mechanical energy from water movement in random directions into electricity, but also could be connected into a network structure for harvesting large-scale energy due to its high scalability, which would further verify our theoretical analysis. We expect that our equivalent circuit model and physical image of the water−solid mode TENG are equally applicable to a general liquid−solid mode TENG, although their rationality and practicality need to be confirmed in future work.

EXPERIMENTAL SECTION

Fabrication of the Water−solid Mode TENG. Figure 1a presents a schematic diagram of the developed water−solid mode TENG, and Figure 1b shows a photograph of the moving part structure. This typical structure was fabricated using a multidielectric layer constructed from polyimide (Kapton) tape and polytetrafluoroethylene (PTFE) films as triboelectric materials. The copper (Cu) layer was deposited on the Kapton tape as electrode, and then they were attached on a 3D printed substrate board (5 × 5 cm^2). Another Cu layer was attached on the bottom of a Petri dish as the second electrode. These two electrodes were connected with each other by a wire to form the external circuit. As depicted in Figure 1a, when the moving part configuration moves up and down in the deionized (DI) water, the potential differences between the two electrodes drive the flow of electrons in the external circuit and thus generate the current.

Fabrication of the Single-Wire TENG and the Three-Dimensional TENG Array. A schematic diagram of the single-wire

https://doi.org/10.1021/acsnano.1c00795
ACS Nano XXXX, XXX, XXX−XXX

TENG is shown in Figure 3a, in which a Cu wire with a diameter of 1.2 mm is utilized as one electrode. As stated before, this special configuration can assist in enhancing efficiency in the utilization of space. When many single-wire TENGs are connected in parallel with each other, a three-dimensional water−solid TENG array can be constructed, and its schematic diagram is presented in Figure 4a.

Characterization and Electrical Measurements. The electric output signals, including the transferred charges (Q_{SC}), and open-circuit voltage (V_{OC}) of these TENG devices, were measured by a digital oscilloscope (Agilent, DSO-X 2014A) and a current preamplifier (Keithley, 6514), respectively.

ASSOCIATED CONTENT

Supporting Information

The Supporting Information is available free of charge at https://pubs.acs.org/doi/10.1021/acsnano.1c00795.

Six videos showing the basic output and capacitor charging of the single-sire TENG (MP4)
(MP4)
(MP4)
(MP4)
(MOV)
(MOV)

The derivation process of the formulas, comparisons of the open-circuit voltage and the short-circuit transferred charge of the single-wire TENG at different water depth, optical images of a single-wire TENG and a TENG array (PDF)

AUTHOR INFORMATION

Corresponding Authors

Khay Wai See − *Institute for Superconducting and Electronic Materials, Australian Institute for Innovative Materials, University of Wollongong, Wollongong, New South Wales 2500, Australia*; Email: kwsee@uow.edu.au

Zhong Lin Wang − *CAS Center for Excellence in Nanoscience, Beijing Key Laboratory of Micro-nano Energy and Sensor, Beijing Institute of Nanoenergy and Nanosystems, Chinese Academy of Sciences (CAS), Beijing 100083, China; College of Nanoscience and Technology, University of Chinese Academy of Sciences, Beijing 100049, China; School of Materials Science and Engineering, Georgia Institute of Technology, Atlanta, Georgia 30332-0245, United States*; orcid.org/0000-0002-5530-0380; Email: zhong.wang@mse.gatech.edu

Xiaolin Wang − *Institute for Superconducting and Electronic Materials, Australian Institute for Innovative Materials and ARC Centre of Excellence in Future Low-Energy Electronics Technologies, University of Wollongong, Wollongong, New South Wales 2500, Australia*; orcid.org/0000-0003-4150-0848; Email: xiaolin@uow.edu.au

Authors

Jing You − *Institute for Superconducting and Electronic Materials, Australian Institute for Innovative Materials, University of Wollongong, Wollongong, New South Wales 2500, Australia*; orcid.org/0000-0002-9001-8049

Jiajia Shao − *CAS Center for Excellence in Nanoscience, Beijing Key Laboratory of Micro-nano Energy and Sensor, Beijing Institute of Nanoenergy and Nanosystems, Chinese Academy of Sciences (CAS), Beijing 100083, China; College of Nanoscience and Technology, University of Chinese Academy of Sciences, Beijing 100049, China*

Yahua He − *Institute for Superconducting and Electronic Materials, Australian Institute for Innovative Materials, University of Wollongong, Wollongong, New South Wales 2500, Australia*

Frank Fei Yun − *Institute for Superconducting and Electronic Materials, Australian Institute for Innovative Materials and ARC Centre of Excellence in Future Low-Energy Electronics Technologies, University of Wollongong, Wollongong, New South Wales 2500, Australia*

Complete contact information is available at: https://pubs.acs.org/10.1021/acsnano.1c00795

Author Contributions

#J.Y., J.S., and Y.H. contributed equally to this work.

Notes

The authors declare no competing financial interest.

ACKNOWLEDGMENTS

This research was partially supported by funding from the Australian Research Council (ARC) through ARC Centre of Excellence in Future Low-Energy Electronics Technologies (CE170100039), Australian Government Global Innovation Linkage Program (GIL 73629), and by the National Key R & D Project from Minister of Science and Technology of China (Grant No. 2016YFA0202704), National Natural Science Foundation of China (Grant Nos. 62001031, 51702018, and 51432005), China Postdoctoral Science Foundation (Grant No. 2019M660766), and Fundamental Research Funds for the Central Universities of China (Grant No. E0E48957). We thank Dr. Tania Silver for her critical reading of the manuscript.

REFERENCES

(1) Lacks, D. J.; Shinbrot, T. Long-Standing and Unresolved Issues in Triboelectric Charging. *Nat. Rev. Chem.* **2019**, *3*, 465−476.
(2) Wang, Z. L.; Wang, A. C. On the Origin of Contact Electrification. *Mater. Today* **2019**, *30*, 34−51.
(3) Wang, Z. L. Triboelectric Nanogenerator (TENG)-Sparking an Energy and Energy and Sensor Revolution. *Adv. Energy Mater.* **2020**, *10*, 2000137.
(4) Shaw, P. E. The Electrical Charges from Like Solids. *Nature* **1926**, *118*, 659−660.
(5) Yun, F. F.; Yu, Z.; He, Y.; Jiang, L.; Wang, Z.; Gu, H.; Wang, X. Voltage-Induced Penetration Effect in Liquid Metals at Room Temperature. *Natl. Sci. Rev.* **2020**, *7*, 366−372.
(6) Moon, J. K.; Song, M. W.; Pak, H. K. Investigation of Surface Charge Density on Solid-Liquid Interfaces by Modulating the Electrical Double Layer. *J. Phys.: Condens. Matter* **2015**, *27*, 194102.
(7) Moon, J. K.; Jeong, J.; Lee, D.; Pak, H. K. Electrical Power Generation by Mechanically Modulating Electrical Double Layers. *Nat. Commun.* **2013**, *4*, 1487.
(8) Favaro, M.; Jeong, B.; Ross, P. N.; Yano, J.; Hussain, Z.; Liu, Z.; Crumlin, E. J. Unravelling the Electrochemical Double Layer by Direct Probing of the Solid/Liquid Interface. *Nat. Commun.* **2016**, *7*, 12695.
(9) Zhan, F.; Wang, A. C.; Xu, L.; Lin, S.; Shao, J.; Chen, X.; Wang, Z. L. Electron Transfer as a Liquid Droplet Contacting a Polymer Surface. *ACS Nano* **2020**, *14*, 17565−17573.
(10) Lin, S.; Xu, L.; Wang, A. C.; Wang, Z. L. Quantifying Electron-Transfer in Liquid-Solid Contact Electrification and the Formation of Electric Double-Layer. *Nat. Commun.* **2020**, *11*, 399.
(11) Nie, J.; Ren, Z.; Xu, L.; Lin, S.; Zhan, F.; Chen, X.; Wang, Z. L. Probing Contact-Electrification-Induced Electron and Ion Transfers at a Liquid-Solid Interface. *Adv. Mater.* **2020**, *32*, 1905696.

(12) Xu, W.; Zheng, H.; Liu, Y.; Zhou, X.; Zhang, C.; Song, Y.; Deng, X.; Leung, M.; Yang, Z.; Xu, R. X.; Wang, Z. L. A Droplet-Based Electricity Generator with High Instantaneous Power Density. *Nature* **2020**, *578*, 392−396.
(13) Wu, H.; Mendel, N.; van den Ende, D.; Zhou, G.; Mugele, F. Energy Harvesting from Drops Impacting onto Charged Surfaces. *Phys. Rev. Lett.* **2020**, *125*, 078301.
(14) Helseth, L. E.; Guo, X. D. Contact Electrification and Energy Harvesting Using Periodically Contacted and Squeezed Water Droplets. *Langmuir* **2015**, *31*, 3269−3276.
(15) Lin, Z. H.; Cheng, G.; Lee, S.; Pradel, K. C.; Wang, Z. L. Harvesting Water Drop Energy by a Sequential Contact-Electrification and Electrostatic-Induction Process. *Adv. Mater.* **2014**, *26*, 4690−4696.
(16) Chatterjee, S.; Burman, S. R.; Khan, I.; Saha, S.; Choi, D.; Lee, S.; Lin, Z. H. Recent Advancements in Solid-Liquid Triboelectric Nanogenerators for Energy Harvesting and Self-Powered Applications. *Nanoscale* **2020**, *12*, 17663−17697.
(17) Tang, W.; Chen, B. D.; Wang, Z. L. Recent Progress in Power Generation from Water/Liquid Droplet Interaction with Solid Surfaces. *Adv. Funct. Mater.* **2019**, *29*, 1901069.
(18) Shi, Q.; Wang, H.; Wu, H.; Lee, C. Self-Powered Triboelectric Nanogenerator Buoy Ball for Applications Ranging from Environment Monitoring to Water Wave Eenergy Farm. *Nano Energy* **2017**, *40*, 203−213.
(19) Choi, D.; Lee, S.; Park, S. M.; Cho, H.; Hwang, W.; Kim, D. S. Energy Harvesting Model of Moving Water inside a Tubular System and Its Application of a Stick-Type Compact Triboelectric Nanogenerator. *Nano Res.* **2015**, *8*, 2481−2491.
(20) Li, X.; Tao, J.; Zhu, J.; Pan, C. A Nanowire Based Triboelectric Nanogenerator for Harvesting Water Wave Energy and Its Applications. *APL Mater.* **2017**, *5*, 074104.
(21) Yang, X.; Chan, S.; Wang, L.; Daoud, W. A. Water Tank Triboelectric Nanogenerator for Efficient Harvesting of Water Wave Energy over a Broad Frequency Range. *Nano Energy* **2018**, *44*, 388−398.
(22) Xia, K.; Tang, H.; Fu, J.; Tian, Y.; Xu, Z.; Lu, J.; Zhu, Z. A High Strength Triboelectric Nanogenerator Based on Rigid-Flexible Coupling Design for Energy Storage System. *Nano Energy* **2020**, *67*, 104259.
(23) Tian, Y.; Wang, Z.; Fu, J.; Xia, K.; Lu, J.; Tang, H.; Rabia, K.; Chen, H.; Zhu, Z.; Zhang, Q.; Zeng, Y. J.; Ye, Z. $Fese_2$/Carbon Nanotube Hybrid Lithium-Ion Battery for Harvesting Energy from Triboelectric Nanogenerators. *Chem. Commun.* **2019**, *55*, 10960−10963.
(24) Lefrou, C.; Fabry, P.; Poignet, J. C. *Electrochemistry: The Basics, with Examples.*; Springer, Verlag: Berlin Heidelberg, 2012.
(25) Brett, C. M. A.; Brett, A. M. O. *Electrochemistry-Principles, Methods and Applications*; Oxford University Press: Oxford, 1993.
(26) Knoblauch, O. Versuche über die Berührungselektrizität. *Z. Phys. Chem.* **1902**, *39*, 225−244.
(27) Shao, J.; Liu, D.; Willatzen, M.; Wang, Z. L. Three-Dimensional Modeling of Alternating Current Triboelectric Nanogenerator in the Linear Sliding Mode. *Appl. Phys. Rev.* **2020**, *7*, 011405.
(28) Shao, J.; Willatzen, M.; Jiang, T.; Tang, W.; Chen, X.; Wang, J.; Wang, Z. L. Quantifying the Power Output and Structural Figure-of-Merits of Triboelectric Nanogenerators in a Charging System Starting from the Maxwell's Displacement Current. *Nano Energy* **2019**, *59*, 380−389.
(29) Shao, J.; Willatzen, M.; Wang, Z. L. Theoretical Modeling of Triboelectric Nanogenerators (TENGs). *J. Appl. Phys.* **2020**, *128*, 111101.
(30) Niu, S.; Wang, Z. L. Theoretical Systems of Triboelectric Nanogenerators. *Nano Energy* **2015**, *14*, 161−192.
(31) Niu, S.; Wang, S.; Lin, L.; Liu, Y.; Zhou, Y. S.; Hu, Y.; Wang, Z. L. Theoretical Study of Contact-Mode Triboelectric Nanogenerators as an Effective Power Source. *Energy Environ. Sci.* **2013**, *6*, 3576−3583.
(32) Levine, S.; Neale, G. H. The Prediction of Electrokinetic Phenomena within Multiparticle Systems. I. Electrophoresis and Electroosmosis. *J. Colloid Interface Sci.* **1974**, *47*, 520−529.
(33) Squires, T. M.; Bazant, M. Z. Induced-Charge Electro-Osmosis. *J. Fluid Mech.* **1999**, *509*, 217−252.
(34) Shao, J.; Jiang, T.; Tang, W.; Chen, X.; Xu, L.; Wang, Z. L. Structural Figure-of-Merits of Triboelectric Nanogenerators at Powering Loads. *Nano Energy* **2018**, *51*, 688−697.
(35) De Gennes, P. G. Wetting: Statics and Dynamics. *Rev. Mod. Phys.* **1985**, *57*, 827−863.
(36) Dharmasena, R. I. G.; Deane, J. H.; Silva, S. R. P. Nature of Power Generation and Output Ooptimization Criteria for Triboelectric Nanogenerators. *Adv. Energy Mater.* **2018**, *8*, 1802190.
(37) Dharmasena, R. D. I. G.; Jayawardena, K. D. G. I.; Mills, C. A.; Deane, J. H. B.; Anguita, J. V.; Dorey, R. A.; Silva, S. R. P. Triboelectric Nanogenerators: Providing a Fundamental Framework. *Energy Environ. Sci.* **2017**, *10*, 1801−1811.
(38) Tandon, V.; Bhagavatula, S. K.; Nelson, W. C.; Kirby, B. J. Zeta Potential and Electroosmotic Mobility in Microfluidic Devices Fabricated from Hydrophobic Polymers: 1. The Origins of Charge. *Electrophoresis* **2008**, *29*, 1092−1101.
(39) Lin, Z. H.; Cheng, G.; Lin, L.; Lee, S.; Wang, Z. L. Water-Solid Surface Contact Electrification and Its Use for Harvesting Liquid-Wave Energy. *Angew. Chem., Int. Ed.* **2013**, *52*, 12545.
(40) Zhu, G.; Su, Y.; Bai, P.; Chen, J.; Jing, Q.; Yang, W.; Wang, Z. L. Harvesting Water Wave Energy by Asymmetric Screening of Electrostatic Charges on a Nanostructured Hydrophobic Thin-Film Surface. *ACS Nano* **2014**, *8*, 6031−6037.
(41) Zhao, X. J.; Zhu, G.; Fan, Y. J.; Li, H. Y.; Wang, Z. L. Triboelectric Charging at the Nanostructured Solid/Liquid Interface for Area-Scalable Wave Energy Conversion and Its Use in Corrosion Protection. *ACS Nano* **2015**, *9*, 7671−7677.
(42) Li, X.; Tao, J.; Wang, X.; Zhu, J.; Pan, C.; Wang, Z. L. Networks of High Performance Triboelectric Nanogenerators Based on Liquid-Solid Interface Contact Electrification for Harvesting Low-Frequency Blue Energy. *Adv. Energy Mater.* **2018**, *8*, 1800705.
(43) Jiang, P.; Zhang, L.; Guo, H.; Chen, C.; Wu, C.; Zhang, S.; Wang, Z. L. Signal Output of Ttriboelectric Nanogenerator at Oil-Water-Solid Multiphase Interfaces and Its Application for Dual-Signal Chemical Sensing. *Adv. Mater.* **2019**, *31*, 1902793.

https://doi.org/10.1021/acsnano.1c00795
ACS Nano XXXX, XXX, XXX−XXX